https://doi.org/10.1038/s44310-024-00006-9

Controlling lasing around exceptional points in coupled nanolasers

Check for updates

Anna Fischer[1,2] ✉, T. V. Raziman[1,3], Wai Kit Ng[1], Jente Clarysse[1], Dhruv Saxena[1], Jakub Dranczewski[1,2], Stefano Vezzoli[1], Heinz Schmid[2], Kirsten Moselund[4,5] & Riccardo Sapienza[1] ✉

Coupled nanolasers are of growing interest for on-chip optical computation and data transmission, which requires an understanding of how lasers interact to form complex systems. The non-Hermitian interaction between two coupled resonators, when excited selectively, can lead to parity-time symmetry, the formation of exceptional points, and subsequently spectral control and increased sensitivity. These investigations have been limited to pump energies close to the lasing threshold, and large or narrow-line lasers. Here, by programmable optical excitation we study two coupled nanolasers significantly above threshold, where mode instability plays an important role. We map the mode evolution around two exceptional points, and observe lasing gaps due to reversed pump dependence which compare well with non-linear theory. Finally, the coupling can be exploited to control the lasing threshold and wavelength, and for frequency switching around the lasing gap. Controlled and integrated nanolasers constitutes a promising platform for future highly sensitive and programmable on-chip laser sources.

Tunable coherent nanoscale light sources are important for many technologies, ranging from on-chip optical computing[1–3] and data transmission[4] to sensing[5] and biophysics[6]. Nanolasers are easier to integrate on-chip and reach GHz modulation[7]. However, fabrication of nanolasers with a specific spectral response is challenging due to intrinsic fabrication imperfections[8–11]. The challenges are exacerbated when many nanolasers are made to interact, to increase power output and functionality due to the complex collective effects[3,12–14].

In coupled nanolasers, parity-time symmetry and its spontaneous breaking at the exceptional point (EP), where eigenmodes of the system coalesce, can be exploited as a powerful tool for post-fabrication spectral control[15–21]. Selectively pumped coupled microdisk lasers are interesting as they provide a wide range of functionalities such as single-mode emission[22–27], optical isolation[28,29], chiral emission[30], and sensing[31–34]. Moreover, the dependence of lasing on gain can be reversed near EPs, resulting in suppression and revival of lasing[35–37].

Yet, the lasing characteristics around EPs have so far mostly been studied for pump energies close to the lasing threshold, where mode competition is minimal and linear coupled mode theory applies[23,26]. Instead, operation well above the threshold is sought for deeper lasing understanding[38] and to exploit new phenomena such as chaotic behaviors and instabilities[39].

Experiments with large microdisks (10−100 μm radii)[22–31], or photonic crystal cavities[18,39] achieve coupling more easily due to narrow linewidths. Instead, in devices of sizes comparable to the wavelength, the effect of coupling is reduced by the low Q-factors, limiting the study of lasing around EPs[40,41].

Here, we study nanoscale coupled InP microdisks, bottom-up grown by epitaxy[42], when excited well above (2×) threshold by selective and programmable illumination. We map the two virtual EPs of the system, and observe the opening of lasing gaps due to reversed pump dependence at the EPs. We demonstrate emission tunability and switching. The experimental findings are confirmed by non-linear coupled-mode theory that includes gain saturation and stability analysis.

Results

The coupled InP microdisk lasers are bottom-up grown, ensuring a defect-free crystal structure with extremely smooth sidewalls corresponding to the ⟨111⟩ facets and high-quality gaps[42,43]. This unique platform reduces cavity losses and makes it possible to reach efficient coupling. The microdisk lasers support few resonant modes within the gain spectral range, owing to their small size, with diameters ranging between 0.5–2 μm and heights between 0.4–1 μm, respectively.

[1]Blackett Laboratory, Department of Physics, Imperial College London, London, UK. [2]IBM Research Europe - Zürich, Säumerstrasse 4, Rüschlikon 8803, Switzerland. [3]Department of Mathematics, Imperial College London, London, UK. [4]Paul Scherrer Institut, Forschungsstrasse 111, Villigen 5232, Switzerland. [5]EPFL, Lausanne 1015, Switzerland. ✉e-mail: anna.fischer@ibm.com; r.sapienza@imperial.ac.uk

The InP microdisks are characterized by a micro photoluminescence and lasing setup. They are excited with a 633 nm, 200 fs-pulsed pump laser. Individual microdisks show single-mode emission with emission wavelengths between 800 and 900 nm, strongly depending on their diameter and height, and with thresholds in the range of 100–700 μJ cm^{-2} pulse^{-1} (Fig. S1). We estimate the Q factor to be below 300 similar to previous works[9]. The low Q factor originates from the small size and leads to a stronger evanescent field outside the disks, which enhances the coupling and enables measurable effects for inter-laser distances up to ~$\lambda/6$. The well-defined gap with smooth sidewalls ensures optimal coupling (Fig. 1a).

We excite the InP microdisk lasers with variable pump on the two disks, that we control using a DMD (digital micromirror device)[44]. The beam is shaped into two half circles with programmable pumping powers P_1 and P_2 (Fig. 1b). The pump power per half circle is varied by defining the fraction of reflecting pixels using a dither function (see Methods). This is an improvement over previous methods, such as covering parts of the pump beam with a knife edge[24], notch filter[23], or simply moving the beam off the device[27], which are inhomogeneous and difficult to control.

The system exhibits a counter-intuitive reversal of the pump dependence of lasing when we keep the pump on disk 2 (P_2) constant and increase the pump P_1 on the other (Fig. 1c)[35–37]. The spectrum evolves, with increasing pump ratio, from single-mode lasing ($P_1/P_2 = 0.56$), to no lasing ($P_1/P_2 = 0.75$), to multimode lasing ($P_1/P_2 = 1$). This observation of reversed pump dependence proves that the microdisks are coupled efficiently. The symmetry of the system ensures the same behavior when P_1 is kept constant, and P_2 varies.

The reversed pump dependence can be well captured by coupled mode theory (see Methods) as shown in Fig. 1d, where each point A-C corresponds to an experimental plot in Fig. 1c. If both microdisks are excited equally (A), the modes of the system split into their real parts (the frequency) while keeping the same imaginary part (the gain/loss), resulting in both modes lasing. The two lasing peaks have different intensities due to frequency-dependent gain in the system, small geometry differences in the disks due to fabrication imperfections, and different emission strengths for bonding and anti-bonding modes. When P_1 is significantly less than P_2 (C), the modes are predominantly split in imaginary part, resulting in single-mode emission. For intermediate values of P_1/P_2, the two modes approach each other in imaginary part, with both imaginary parts going below the threshold for a range of ratios (B). For a zero-detuned system (gray dashed line), where $\omega_1 = \omega_2 = \omega_0$, the two modes meet at an exceptional point (EP), where both the eigenvalues and eigenvectors coalesce (identified by the arrow in Fig. 1d)[15–19]. At the EP, the system is highly sensitive to perturbations showing strong responses in the spectral features[31–34]. Slight detuning of the resonant frequencies (colored line) $\omega_i = \omega_0 \pm \delta$ produces an avoided crossing around the zero-detuning EP, which still has similar implications on the spectral response as an EP.

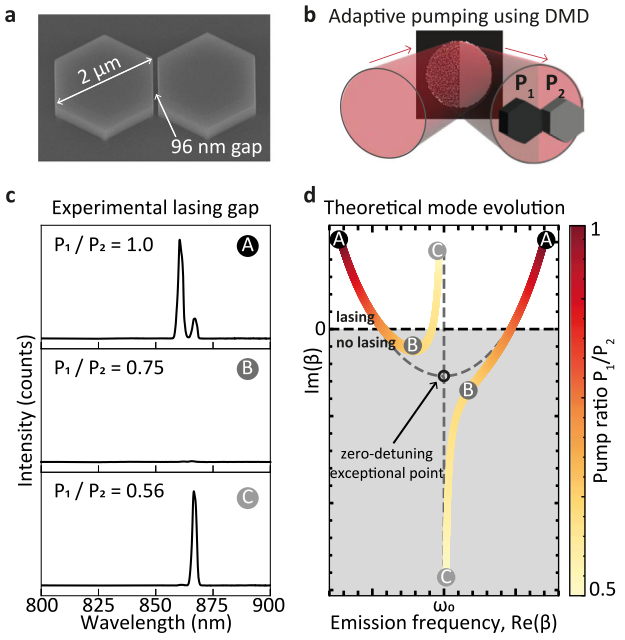

Fig. 1 | Counter-intuitive lasing behavior in coupled microdisk lasers. a SEM image of two coupled bottom-up grown InP microdisk lasers with 2 μm diameter and 96 nm gap. **b** Schematic of the DMD setup and pattern used for selective pumping, where the uniform beam is reflected from the DMD and shaped into two half circles with powers P_1 and P_2. **c** Three emission spectra illustrating the lasing gap under selective pumping of coupled InP microdisk lasers. P_2 = 163 μJ cm^{-2} pulse^{-1} for all three acquired spectra, while P_1 is increased from bottom to top. **d** Evolution of real and imaginary parts of mode eigenvalues based on linear coupled mode theory under selective pumping. In the experimental spectrum, the modes have different intensities due to effects such as mode competition and non-equal losses of the disks, which are not included in coupled mode theory.

We can obtain a complete map of the lasing landscape including the behavior far above threshold by varying P_1 and P_2 independently (Fig. 2). The intensities of mode 1 (blue shading) and mode 2 (orange shading) are shown for both uncoupled (top panels) and coupled (bottom panels) systems, based on theoretical predictions (left panels) and experimental results (right panels).

When two resonators are *uncoupled*, each laser is unaffected by the pump on the other disk (Fig. 2a). Therefore, the system has one lasing mode per disk. A mode reaches threshold when it is pumped sufficiently to offset the losses, making the threshold lines (blue and orange lines) parallel to the pump axes. Lasing measurements of uncoupled InP microdisks reproduce the theoretical threshold behavior (Fig. 2b, for 2 μm diameter, 680-nm gap device, SEM image in Fig. S3). The lasing spectrum is shown in the inset of Fig. 2b for different pump powers (dots in the main figure).

When two resonators are *coupled*, the modes become delocalized across the two disks, which makes lasing action dependent on both pump powers $P_{1,2}$ and the threshold lines are no longer straight lines aligned along the pump axis (Fig. 2c, d). We first analyze the lasing action for pump powers close to the lasing threshold with linear coupled mode theory (see Methods). We calculate the theoretical modes for resonators with slight frequency detuning ($\delta/\kappa = 0.2$) to better reflect the experimental conditions (see later). When the pump powers on both disks become close to the lasing threshold, the coupling transfers gain from the more highly pumped disk to the other. As a result, the threshold of the more pumped disk increases with respect to the uncoupled value while that of the less pumped disk decreases, pulling the threshold lines towards each other (solid lines in Fig. 2c). In a zero-detuned system, the threshold lines would merge into a single segment, known as the parity-time symmetry line[16], where both modes have the same threshold (Fig. S7). At the ends of the parity-time symmetry line lie the EPs of the zero-detuned system, where the eigenmodes coalesce. Frequency detuning prevents this coalescence and instead creates avoided crossings around the zero-detuning EPs (black crosses in Fig. 2c).

Above threshold, gain saturation and mode competition modify the lasing behavior. This can be captured by extending linear coupled mode theory to include gain saturation[38,45] and stability analysis[46]. With this nonlinear model, we compute the mode intensities above threshold (see Supplementary Information section SIII). When one mode is above threshold, the second mode (solid line, Fig. 2c) appears at a higher threshold than predicted by linear coupled mode theory (dashed line). Between the solid and dashed lines, the second mode is unstable, and therefore, only the mode with the higher gain lases.

Experimental threshold lines of coupled InP microdisks follow the features predicted by theory (Fig. 2d, for 2 μm diameter, 96 nm gap device). The indicated threshold lines are a combination of calculated values (orange and blue dots) and guides (orange and blue lines). The calculated values were obtained by finding steep increases in emission intensity marking the inversion point typical for lasing thresholds in LL-curves (Fig. S5). When the pump power is similar in both disks, the effect of increase in threshold, with a similar shape as predicted by theory, is observed (orange and blue dots in

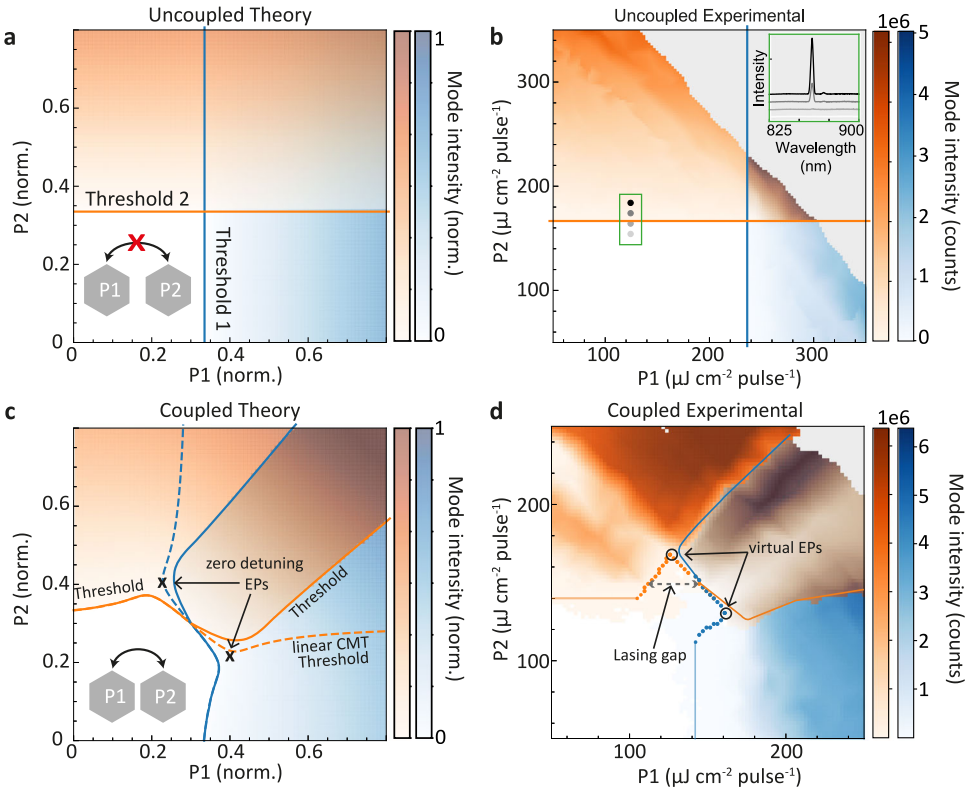

Fig. 2 | Mode thresholds become highly co-dependent in a coupled system. **a** Theoretical mode landscape as a function of pumping power $P_{1,2}$ of two uncoupled microdisks (schematic in inset) showing how the threshold of each disk is independent of pumping on the other disk and only dependent on the intrinsic losses which are set to $\gamma_1 = \gamma_2 = \gamma = 0.3$. **b** Experimental mode landscape of two uncoupled InP microdisks with 2 μm diameter and 680-nm gap showing the independent thresholds of the two microdisks. The green inset shows emission spectra at four pump powers (fixed $P_1 = 74$ μJ cm^{-2} pulse^{-1}; $P_2 = 154$, 164, 174, and 184 μJ cm^{-2} pulse^{-1}), indicated as grayscale dots in main plot. **c** Theoretical mode landscape of two coupled microdisks (schematic in inset) with slight frequency detuning $\delta = 0.02$, coupling $\kappa = 0.1$, and losses $\gamma = 0.3$. The threshold lines of the two modes are clearly affected by increased pump power on the other disk. The two **x** mark where EPs would lie in a zero-detuned system. Due to detuning, avoided crossings are visible around the EPs. An instability region separates the theoretical threshold (dashed line) from the actual onset of the second mode (solid lines). **d** Experimental mode landscape of two coupled InP microdisks with 2 μm diameter and 96-nm gap. The indicated threshold lines are a combination of calculated values (dots) and estimated visual guides (lines). The coupling results in two virtual EPs around which lasing gaps open (gray dashed arrow). For all plots, the intensity of the mode is given by the color (see color bars). White: below threshold, gray area: no data.

Fig. 2d). The threshold lines lie nearly on top of each other in this region due to the large coupling between the disks. The black circles indicate the position of so-called "virtual" EPs. These points are the minima of the avoided crossings at the zero-detuning EPs and represent the closest a physical system can come to an EP without active detuning modulation[39]. The experimental onset of the second lasing mode above threshold follows the theory and confirms the need for non-linear coupled mode theory above threshold. The threshold of mode 1 (blue line) for a device already lasing in mode 2 (orange shading) follows a straight line with positive slope above threshold. At very high pumping powers, $P_2 > 250$ μJ cm^{-2} pulse^{-1}, the threshold of mode 2 (orange line) deviates from the theoretical prediction, which we attribute to non-linear interactions with higher-order modes in the system.

The virtual EPs allow us to estimate the coupling in the system, as their distance is equal to the coupling factor $\kappa = 18$ μJ cm^{-2} pulse^{-1} and $\kappa/\gamma = 0.13$, where γ are the losses of the microdisks and equal to the threshold $P_{th} \approx 140$ μJ cm^{-2} pulse^{-1}. Using the Q factor of the device, the coupling constant could be given in THz, and the proportion of mode-splitting due to coupling versus detuning obtained. Estimates can be found in the Supplementary Information (section SIV).

If the coupling is larger than the laser linewidth, a lasing gap, where the pump dependence is reversed[35–37], opens near the virtual EPs (Fig. 2d, dashed line).

The corresponding spectra in Fig. 3a clearly show the reversal in pump dependence, where the lasing stops even though the excitation power increases. This is followed by the lasing gap and a revival of the lasing at shifted frequencies (Fig. 3a).

The lasing gap Δ, defined as the pump separation between the two lasing actions, narrows for increased P_2 powers and when it closes, for a pump $P_2 = 186$ μJ cm^{-2} pulse^{-1}, the system reaches the "virtual" EP as shown in Fig. 3b (see Supplementary Information section SV for the second virtual EP of the system). The large coupling between the microdisks, which is the result of narrow and high-quality gaps between the disks, enables to access large lasing gaps of up to 30% of the lasing threshold (Fig. 3b).

Around the lasing gap, the emission wavelength shifts, as the mode eigenvalues start to split in their real part. This wavelength shift is proportional to the lasing gap size and increases for larger gaps (Fig. 3c). The gradient of this relation depends on the coupling strength, of the system. For stronger coupling, the wavelength shifts more around the lasing gap as the splitting of the real parts of the eigenvalue is enhanced.

When keeping P_2 at 152 μJ cm^{-2} pulse^{-1}, a wavelength shift of 3 nm is observed between spectra slightly before (light blue in Fig. 4a) and after (dark blue) the lasing gap. As a reference, this shift is 10 times larger than a shift due to carrier plasma effect at similar pump powers and also ensures similar output intensities (Supplementary Information section SVI)[47].

The shift close to the virtual EP can be exploited to rapidly switch the laser emission frequency. We demonstrate low-power (0.97(2) μW) switching with $\Delta\lambda = 5$ nm for a lasing peak with 1 nm FWHM, as plotted in Fig. 4b. The switching is very stable with a standard deviation of only 0.07 nm, which is mostly attributed to fluctuations in the pump laser.

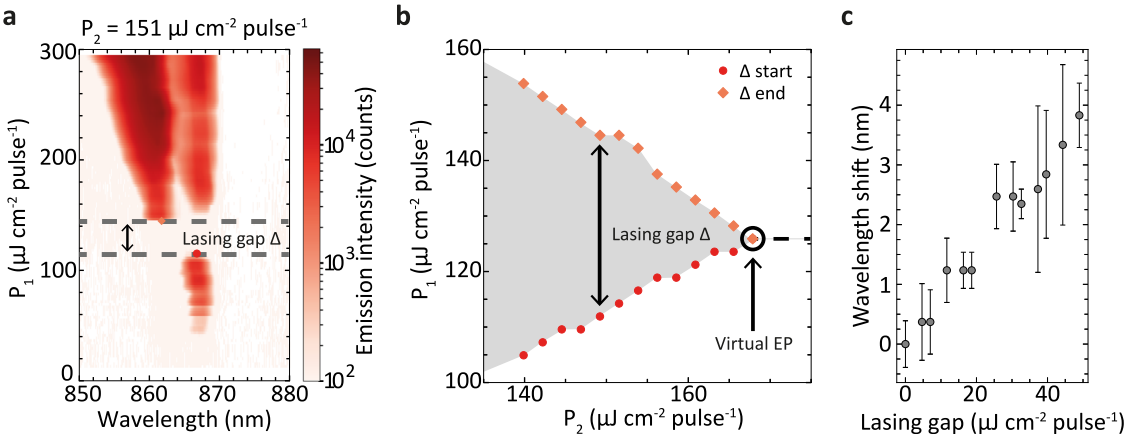

Fig. 3 | The lasing gap narrows under increased P_1 and closes at a "virtual" EP. **a** Pump power on disk 1 (P_1) versus emission wavelength for constant P_2 of 151 μJ cm^{-2} pulse^{-1}. The colourbar indicates the emission intensity. While P_1 is increased, the lasing stops and then resurfaces at a shifted frequency resulting in a counter-intuitive lasing gap. **b** The lasing gap decreases under increased P_2. When the lasing gap closes, a "virtual" (due to experimentally inherent detuning) EP at the avoided crossing is reached. **c** Wavelength shift across the lasing gap versus lasing gap size.

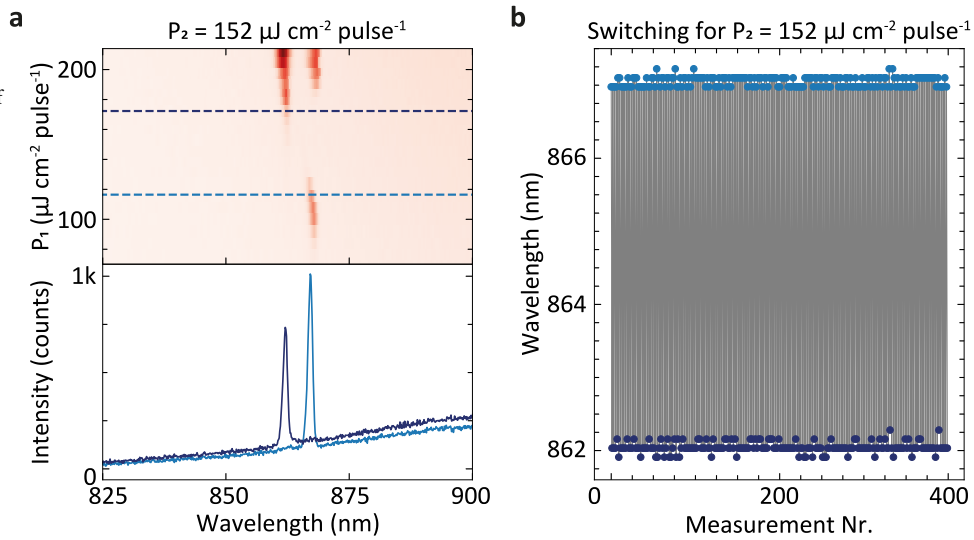

Fig. 4 | The lasing gap enables stable, low-power wavelength switching. **a** The upper colourmap shows P_1 versus emission wavelength plot for constant P_2 of 152 μJ cm^{-2} pulse^{-1}, with the darkness of the red indicating the emission intensity. Two spectra before (light blue, P_1 = 117 μJ cm^{-2} pulse^{-1}) and after (dark blue, P_1 = 172 μJ cm^{-2} pulse^{-1}) the lasing gap are shown in the lower plot, and their position in the upper plot is indicated by dashed lines. **b** Low-power (0.97(2) μW) and stable switching between two emission wavelengths around the lasing gap with $\Delta\lambda$ = 5 nm and $\Delta\lambda$/FWHM = 1.7.

The pump power regime chosen for Fig. 4b results in intensity modulation of 9.2 (10.5) dB for the lower (higher) wavelength peak, for the application of a small ΔP around 1 μW. This value can be significantly increased by optimizing the P_1 and P_2 powers. At higher powers, other switching effects, such as switching from single-mode to multi-mode emission, are possible (see Supplementary Information section SVII).

Conclusion

To conclude, we studied bottom-up grown coupled InP microdisk lasers through above threshold and selective lasing spectroscopy. Programmable illumination allows for precise control of the lasing mode behavior around two virtual EPs and access functionalities such as single-mode emission, reversed pump dependence, increased sensitivity, and switching, in a single programmable device. The resulting lasing operation is well explained by non-linear coupled-mode theory that includes gain saturation and stability analyses. The very low-power wavelength switching around the lasing gap is promising for on-chip applications in information processing. It could also enable fast switching as the laser dynamics do not rely on ns-slow non-radiative recombination processes. Such coupled on-chip resonators could be a promising basis for new types of on-chip optical switching, communication[4], sensing[5], and machine learning application[1,3,48].

Materials and methods

Coupled mode theory

We model the coupled microdisk laser system around threshold through coupled mode theory. Coupled mode theory is an established theory for evanescently coupled microdisk lasers[16,17,23,38]. We consider two single-mode resonators ($i = 1, 2$) with resonant frequencies $\tilde{\omega}_i = \omega_i - i\gamma_i$, where ω_i is the real frequency and γ_i is the imaginary part corresponding to the loss. The resonators are coupled by a real coupling factor κ. We pump the resonators with pump P_i. When the system is around threshold we can neglect non-linear gain saturation, and the steady-state behavior is described by the linear 2 × 2 matrix eigenvalue equation,

$$\begin{bmatrix} \omega_1 - i\gamma_1 + iP_1 & \kappa \\ \kappa & \omega_2 - i\gamma_2 + iP_2 \end{bmatrix} \begin{bmatrix} \tilde{\psi}_1 \\ \tilde{\psi}_2 \end{bmatrix} = \tilde{\omega} \begin{bmatrix} \tilde{\psi}_1 \\ \tilde{\psi}_2 \end{bmatrix} \quad (1)$$

The eigenvalues $\tilde{\omega}$ of Eq. (1) are the modes of the coupled system, where Re($\tilde{\omega}$) is the emission frequency and is the the loss/gain of the system. For Im($\tilde{\omega}$) > 0 (<0) the system is above (below) the lasing threshold of Im($\tilde{\omega}$) = 0.

For the above threshold solutions, Eq. (1) becomes non-linear, and we included gain saturation to find the solutions (see Supplementary Information section SIII).

Microdisk fabrication

The bottom-up grown WZ InP microdisks are fabricated as reported in[42]. The crystal growth and WZ structure are induced by 110-oriented trenches in a 300 nm SiO_2 layer on a standard InP (111)A substrate. The trenches are fabricated using e-beam lithography (EBL) and reactive ion etching (RIE). InP is grown inside the trenches through metal-organic vapor phase epitaxy (MOVPE) resulting in fins, that are the base of the microdisks and define their diameter. Once the InP reaches the top of the trenches, zipper-induced epitaxial lateral overgrowth (ELO) extends the InP laterally over the SiO_2 until the base of the hexagonal microdisk is formed. The growth then occurs vertically to form InP microdisks with flat crystalline sidewalls.

Optical measurements

The InP microdisks are characterized in a micro photoluminescence setup. They are pumped with a 633 nm, 200 fs-pulsed laser at 100 kHz. The pump beam is focused on the sample using a ×100 objective. The microdisks are excited from above, and their emitted light is also collected from above through the same objective. The emission spectra are measured in a Princeton Instruments spectrometer. We shape the pump beam into two half circles with independently adjusted powers by reflection off a DMD that consists of 1280 × 800 addressable mirror pixels. As single DMD pixels are not resolved due to their small size, turning off a fraction of the pixels reduces the power of the beam. To achieve uniform pixel distribution, we used Floyd-Steinberg's error diffusion dither algorithm incorporated in MATLAB. We measure the exact power on each disk with a calibrated powermeter that measures light reflected off a glass slide. The glass slide is located before the objective, and the ratio between the power at the powermeter and sample location was measured to calibrate the powermeter. To obtain the power on each disk separately, the single beam halves were projected, and the power obtained before the full pattern projection and spectrum measurement.

Data availability

The data used is available in the Zenodo repository: https://doi.org/10.5281/zenodo.10683232.

Received: 22 December 2023; Accepted: 26 January 2024;
Published online: 02 May 2024

References

1. Brunner, D. & Psaltis, D. Competitive photonic neural networks. *Nat. Photonics* **15**, 323–324 (2021).
2. Shen, Y. et al. Deep learning with coherent nanophotonic circuits. *Nat. Photonics* **11**, 441–446 (2017).
3. Tirabassi, G., Ji, K., Masoller, C. & Yacomotti, A. M. Binary image classification using collective optical modes of an array of nanolasers. *APL Photonics* **7**, 090801 (2022).
4. Wang, Z. et al. Novel light source integration approaches for silicon photonics. *Laser Photonics Rev.* **11**, 1700063 (2017).
5. Zhong, Q. et al. Sensing with exceptional surfaces in order to combine sensitivity with robustness. *Phys. Rev. Lett.* **122**, 153902 (2019).
6. Caixeiro, S. et al. Local sensing of absolute refractive index during protein-binding using microlasers with spectral encoding. *Adv. Opt. Mater.* **n/a**, 2300530 (2023).
7. Xu, C., Hayenga, W. E., Christodoulides, D. N., Khajavikhan, M. & LiKamWa, P. Direct modulation of electrically pumped coupled microring lasers. *Opt. Express* **30**, 1143–1151 (2022).
8. Gil-Santos, E. et al. Scalable high-precision tuning of photonic resonators by resonant cavity-enhanced photoelectrochemical etching. *Nat. Commun.* **8**, 14267 (2017).
9. Mauthe, S. et al. InP-on-Si optically pumped microdisk lasers via monolithic growth and wafer bonding. *IEEE J. Sel. Top. Quantum Electron.* **25**, 1–7 (2019).
10. Tiwari, P. et al. Single-mode emission in InP microdisks on Si using Au antenna. *ACS Photonics* **9**, 1218–1225 (2022).
11. Dranczewski, J. et al. Plasma etching for fabrication of complex nanophotonic lasers from bonded InP semiconductor layers. *Micro Nano Eng.* **19**, 100196 (2023).
12. Choi, J.-H. et al. Room temperature electrically pumped topological insulator lasers. *Nat. Commun.* **12**, 3434 (2021).
13. Qiao, X. et al. Higher-dimensional supersymmetric microlaser arrays. *Science* **372**, 403–408 (2021).
14. Lepri, S., Trono, C. & Giacomelli, G. Complex active optical networks as a new laser concept. *Phys. Rev. Lett.* **118**, 123901 (2017).
15. Bender, C. M. & Boettcher, S. Real spectra in non-Hermitian Hamiltonians having PT symmetry. *Phys. Rev. Lett.* **80**, 5243–5246 (1998).
16. Özdemir, Ş. K., Rotter, S., Nori, F. & Yang, L. Parity–time symmetry and exceptional points in photonics. *Nat. Mater.* **18**, 783–798 (2019).
17. El-Ganainy, R. et al. Non-Hermitian physics and PT symmetry. *Nat. Phys.* **14**, 11–19 (2018).
18. Hamel, P. et al. Spontaneous mirror-symmetry breaking in coupled photonic-crystal nanolasers. *Nat. Photonics* **9**, 311–315 (2015).
19. Miri, M.-A. & Alù, A. Exceptional points in optics and photonics. *Science* **363**, 42 (2019).
20. Li, A. et al. Exceptional points and non-hermitian photonics at the nanoscale. *Nat. Nanotechnol.* **18**, 706–720 (2023).
21. Feng, L., El-Ganainy, R. & Ge, L. Non-hermitian photonics based on parity-time symmetry. *Nat. Photonics* **11**, 752–762 (2017).
22. Feng, L., Wong, Z. J., Ma, R.-M., Wang, Y. & Zhang, X. Single-mode laser by parity-time symmetry breaking. *Science* **346**, 972–975 (2014).
23. Hodaei, H., Miri, M.-A., Heinrich, M., Christodoulides, D. N. & Khajavikhan, M. Parity-time–symmetric microring lasers. *Science* **346**, 975–978 (2014).
24. Hodaei, H. et al. Parity-time-symmetric coupled microring lasers operating around an exceptional point. *Opt. Lett.* **40**, 4955 (2015).
25. Wang, H., Liu, S., Chen, L., Shen, D. & Wu, X. Dual-wavelength single-frequency laser emission in asymmetric coupled microdisks. *Sci. Rep.* **6**, 38053 (2016).
26. Hodaei, H. et al. Design considerations for single-mode microring lasers using parity-time-symmetry. *IEEE J. Select. Top. Quantum Electron.* **22**, 12–18 (2016).
27. Liu, G. et al. Single-mode lasing with spontaneous symmetry breaking from a perovskite microdisk dimer. *ACS Photonics* **10**, 43–48 (2023).
28. Peng, B. et al. Parity–time-symmetric whispering-gallery microcavities. *Nat. Phys.* **10**, 394–398 (2014).
29. Chang, L. et al. Parity–time symmetry and variable optical isolation in active–passive-coupled microresonators. *Nat. Photonics* **8**, 524–529 (2014).
30. Hayenga, W. E. et al. Direct generation of tunable orbital angular momentum beams in microring lasers with broadband exceptional points. *ACS Photonics* **6**, 1895–1901 (2019).
31. Chen, W., Kaya Özdemir, Ş., Zhao, G., Wiersig, J. & Yang, L. Exceptional points enhance sensing in an optical microcavity. *Nature* **548**, 192–196 (2017).
32. Wiersig, J. Enhancing the sensitivity of frequency and energy splitting detection by using exceptional points: application to microcavity sensors for single-particle detection. *Phys. Rev. Lett.* **112**, 203901 (2014).
33. Zhong, Q., Christodoulides, D. N., Khajavikhan, M., Makris, K. G. & El-Ganainy, R. Power-law scaling of extreme dynamics near higher-order exceptional points. *Phys. Rev. A* **97**, 020105 (2018).
34. Wiersig, J. Review of exceptional point-based sensors. *Photonics Res.* **8**, 1457–1467 (2020).

35. Liertzer, M. et al. Pump-induced exceptional points in lasers. *Phys. Rev. Lett.* **108**, 173901 (2012).
36. Brandstetter, M. et al. Reversing the pump dependence of a laser at an exceptional point. *Natu. Commun.* **5**, 4034 (2014).
37. Peng, B. et al. Loss-induced suppression and revival of lasing. *Science* **346**, 328–332 (2014).
38. Benzaouia, M., Stone, A. D. & Johnson, S. G. Nonlinear exceptional-point lasing with ab initio Maxwell–Bloch theory. *APL Photonics* **7**, 121303 (2022).
39. Ji, K. et al. Tracking exceptional points above laser threshold. *Nat commun.* **14**, 8304 (2022).
40. Ishii, S. & Baba, T. Bistable lasing in twin microdisk photonic molecules. *Appl. Phys. Lett.* **87**, 181102 (2005).
41. Nakagawa, A., Ishii, S. & Baba, T. Photonic molecule laser composed of GaInAsP microdisks. *Appl. Phys. Lett.* **86**, 041112 (2005).
42. Staudinger, P. et al. Wurtzite InP microdisks: from epitaxy to room-temperature lasing. *Nanotechnology* **32**, 075605 (2020).
43. Schmid, H. et al. Template-assisted selective epitaxy of III–V nanoscale devices for co-planar heterogeneous integration with Si. *Appl. Phys. Lett.* **106**, 233101 (2015).
44. Saxena, D. et al. Sensitivity and spectral control of network lasers. *Nat. Commun.* **13**, 6493 (2022).
45. Santos, E. P. et al. Gain clamping in random lasers. *Laser Phys. Lett.* **18**, 125002 (2021).
46. Strogatz, S. H. Nonlinear dynamics and chaos: with applications to physics, biology, chemistry, and engineering, 2nd edn (CRC Press, Boca Raton, 2019).
47. Bennett, B., Soref, R. & Del Alamo, J. Carrier-induced change in refractive index of InP, GaAs and InGaAsP. *IEEE J. Quantum Electron.* **26**, 113–122 (1990).
48. Porte, X. et al. A complete, parallel and autonomous photonic neural network in a semiconductor multimode laser. *J. Phys. Photonics* **3**, 024017 (2021).

Acknowledgements

AF, JD, HM, and KM acknowledge support from the EU ITN EID project CORAL (GA no. 859841). TVR, DS, and RS acknowledge support from The Engineering and Physical Sciences Research Council (EPSRC), grant number EP/T027258. WKN acknowledges the research support funded by the President's PhD Scholarships from Imperial College London. SV acknowledges support from EPSRC–EP/X52556X/1. We thank Philipp Staudinger and the Cleanroom Operations Team of the Binnig and Rohrer Nanotechnology Center (BRNC) for sample fabrication together with HS.

Author contributions

Conceptualization: AF, RS, WKN, TVR, DS, JC; optical measurements: AF; optical setup: SV, DS, WKN, AF, JD; theory: TVR, AF, JC, WKN; data analysis: AF, TVR; fabrication: HS, KM; visualization: AF, TVR, JC; funding acquisition: RS, KM; project administration: RS, KM; supervision: RS; writing (original draft): AF; writing (review and editing): AF, TVR, RS, SV, DS, KM, HS, JD, WKN, JC.

Competing interests

The authors declare no competing interests.

Additional information

Supplementary information The online version contains supplementary material available at https://doi.org/10.1038/s44310-024-00006-9.

Correspondence and requests for materials should be addressed to Anna Fischer or Riccardo Sapienza.

Reprints and permissions information is available at http://www.nature.com/reprints

Publisher's note Springer Nature remains neutral with regard to jurisdictional claims in published maps and institutional affiliations.

Open Access This article is licensed under a Creative Commons Attribution 4.0 International License, which permits use, sharing, adaptation, distribution and reproduction in any medium or format, as long as you give appropriate credit to the original author(s) and the source, provide a link to the Creative Commons licence, and indicate if changes were made. The images or other third party material in this article are included in the article's Creative Commons licence, unless indicated otherwise in a credit line to the material. If material is not included in the article's Creative Commons licence and your intended use is not permitted by statutory regulation or exceeds the permitted use, you will need to obtain permission directly from the copyright holder. To view a copy of this licence, visit http://creativecommons.org/licenses/by/4.0/.

© IBM, under exclusive licence to Springer Nature Limited 2024